ISSN: 0975-833X

Available online at http://www.journalcra.com

International Journal of Current Research
Vol. 17, Issue, 08, pp.34179-34190, August, 2025
DOI: https://doi.org/10.24941/ijcr.49315.08.2025

INTERNATIONAL JOURNAL OF CURRENT RESEARCH

RESEARCH ARTICLE

SPRAY PYROLYTIC LAYER MODIFICATION OF GLASS REINFORCED POLYMER SUBSTRATE USING GRAPHENE AND GRAPHITE BLEND

Kenechi Ijeoma OJEMENI*, Johnson Olumuyiwa AGUNSOYE and Henry E MGBEMERE

Department OF Metallurgical and Materials Engineering, University of Lagos, Akoka, Yaba, Lagos

ARTICLE INFO

Article History:
Received 11th May, 2025
Received in revised form
24st June, 2025
Accepted 19th July, 2025
Published online 20th August, 2025

Keywords:
Graphene, Graphite, Glass Reinforced Polymer, Layer Modification, Pipeline.

***Corresponding author:**
Kenechi Ijeoma OJEMENI

ABSTRACT

Conveyance of crude oil is usually done using carbon steel pipes due to their high strength and electrical conductivity. However, carbon steel is prone to severe corrosion both internally and externally. Hence, it becomes necessary to develop suitable, lightweight, cost-effective, and electrically conductive materials that can serve as alternatives to carbon steel pipeline sections in the oil and gas industry. This study investigates the adaptability of nanoparticle-sized graphene and graphite-coated GRP (Glass Reinforced Polymers) as substitutes for steel in corrosion control and pipeline rehabilitation. The coating process employed low-temperature spray pyrolysis (50–60 °C) to deposit nanoparticle graphene and carbonized graphite on GRP substrates of $50 \times 10 \times 2$ mm dimensions. Single- and double-layer coatings were applied using graphene-graphite blend ratios of 1:0.5 and 1:1. Electrical resistance was measured using an LCR meter, from which electrical conductivity was calculated. The samples were characterized using SEM, XRD, FTIR, and thermal analysis (TGA), while hardness was evaluated using the Rockwell method (HLD). Results showed that the GRP sample with a double-layer 1:1 graphene: graphite blend had the highest hardness (59.33 HLD), while the GRP with single-layer graphene coating recorded the highest electrical conductivity of 1.8×10^{-6} S/m. TGA revealed improved thermal stability in GRP samples, with glass transition temperatures (Tg) near 400 °C. Image J analysis of SEM images showed that moderate grain sizes (2–4 μm²) correlated strongly with improved wear resistance and conductivity. Wear tests confirmed that the 1-0.5D hybrid sample had the lowest wear rate and volume loss, while performance indexing ranked G-S (Graphene Single Layer) as the best all-around GRP performer. Tensile testing demonstrated significant improvements in strength, stiffness, and ductility, with tensile stresses above 23 MPa in coated GRP samples. A mathematical model was also developed to predict electrical conductivity as a function of coating thickness. Additionally, CP modelling demonstrated that introducing a non-conductive GRP section in an ICCP-protected pipeline causes localized under protection, which can be mitigated using optimized bypass wire design. In conclusion, this study establishes that graphene and graphite coatings, applied via spray pyrolysis, enhance the electrical, mechanical, and thermal properties of GRP. Among these, GRP composites coated with graphene—especially G-S and 1-0.5D—offer a promising, multifunctional alternative for steel in pipeline repair, leak mitigation, and corrosion control applications in the oil and gas industry.

Citation: Kenechi Ijeoma OJEMENI, Johnson Olumuyiwa AGUNSOYE and Henry E MGBEMERE. 2025. "Spray Pyrolytic Layer Modification of Glass Reinforced Polymer Substrate Using Graphene and Graphite Blend". *International Journal of Current Research, 17, (08), 34179-34190.*

INTRODUCTION

Conductive pipes and composite coil tubings have introduced innovative installation techniques in offshore drilling (1). Piping and pipeline applications using composites represent a frontier in technological advancement in materials science and engineering (2). Various techniques, including layer modification, have been developed to enhance the electrical conductivity of composites. Among layer materials, graphene stands out due to its high electrical conductivity, thin film-forming ability, thermal stability, and mechanical strength (3,4). A significant problem the oil and gas industry faces is the design and selection of suitable piping materials to ensure longevity in service and cost-effective corrosion management. Besides conventional steel pipes, polymeric composites have been found promising for their non-corrosive nature (5). Although several glass fibre-reinforced thermoplastic composite pipes have been developed, the challenge is the applicability of these pipes in certain operations where electrical conductivity is of primary importance (6). Electrical conductivity is required when cathodic protection is used to protect buried pipes. The cathodic protection system supplies current through the electrolyte (soil, water, etc.) to the pipe, which is conducted through the pipe and returned to the cathodic protection system. Conductive polymer matrix composites are engineered by dispersing conductive phases such as graphene or carbon fibers in polymeric resins, resulting in non-metallic anisotropic behaviour with notable electrical, magnetic, and thermal properties (7-10). The demand for conductive materials with tailorable

mechanical properties across industries like oil and gas, aerospace, automotive, and electronics has driven extensive research efforts. These have led to the development of conductive composite materials that address the challenges faced by these industries (11,12). Currently, the oil and gas industry demands certain technical, technological, and economic requirements that are not fully met with the use of metallic materials. Specifically, in the aspect of pipeline construction, to combat corrosion, materials employed in the construction of pipes are required to be corrosion-resistant and electrochemically suitable for the cathodic protection of steel pipes. Using GRP pipes with a combination of chemical stability and high electrical conductivity will reduce corrosion problems in the industry. This research focuses on layer modification through the spray pyrolysis of graphene particulates to improve the electrical conductivity of composite pipes.

MATERIALS AND METHODS

Sample Preparation: The materials used in the course of this research include pure glass reinforced polymer (GRP) samples, graphite powder, graphene powder, and polyvinyl alcohol (PVA), as the binder. The GRP samples were first ground with grit papers of grit size 80 to roughen the surface. Afterward, they were cleaned to remove impurities like dirt or grease from the surface using a solution of acetone. The samples were put in a beaker with 100 ml of acetone and left in the solution for 10 minutes. Afterward, the acetone was discarded, and the samples were put in a beaker of 100 ml of distilled water and placed in the sonicator for another 10 minutes. The samples were then placed in the sterilizing oven to dry at 50 °C for 30 minutes. The coating materials were prepared by mixing the graphite powder and the graphene powder with a solution of PVA (which serves as the binder). Three different coating solutions were prepared, each having a different mass ratio of graphene and graphite, while the ratio of the binder was kept constant in all three solutions. The mass ratio of graphene to graphite in the coating solutions is shown in Table 1. The composition was stirred in a magnetic stirrer at 80 ^{o}C for 4 hours.

Table 1. Various compositions used

Control (PVC)	1 Layer deposit using graphene (G-S)	2 Layer deposition of graphene (G-D)	Deposition of one Layer graphene + local graphite 1:1 (1-1S)
Deposition of two-layer graphene + Local graphite 1:1 (1-1D)	Deposition of one Layer graphene + local graphite 1:0.5 (1-0.5S)	Deposition of two-layer graphene + Local graphite 1:0.5 (1-0.5D)	

From the literature, the use of the hot pyrolysis technique is a standard method for coating materials with high melting temperatures (>400 °C), such as metals, brass, and bronze. Therefore, to avoid incipient melting, this study used a lower-temperature pyrolysis technique (between 50 °C and 60 °C). The Nebulizer spray pyrolysis technique (NSPT) was used to deposit the prepared precursor solutions on a GRP substrate. The precursor solution is atomized into tiny droplets and then transported on top of the heated substrate head with some initial velocity. This is the basis for the operation of the Nebulizer Spray Pyrolysis Machine. The single-phase connection electric motor receives electricity from an external source and transforms it into mechanical energy, which is then transferred to the pulley system via a conveyor belt. The rotation of the rod causes the pulley that comes into contact with it to rotate. The conveyor belt transfers the pulley's mechanical action to the compressor, causing the compressor to start. Both a suction and a discharge valve are included in the compressor. Air is drawn from the environment by the suction valve and then discharged through the 2 cm-diameter host into the tank's input nozzle by the discharge valve, which then delivers the air to the storage tank, which is a cylindrical tank. The compressor air tank's compressed air, measured using a pressure gauge to be at around 3 bars, is permitted to enter the filter via the exit nozzle and filter out pollutants such as dust, water, and oil. Subsequently, the atomizer receives the filtered air and atomizes the precursor solution into smaller droplets. After that, they are sprayed onto the GRP substrate and allowed to dry at room temperature.

Testing and Characterisation: The thickness of the coatings was measured by cutting each sample into two halves (perpendicular to its length) using a TechCut 4 low-speed saw from Allied High Tech. Productions Inc. The thickness of the coatings was measured using a digital thickness gauge, and the values were calculated by taking the mean of three thickness values on each sample. An LCR (Inductance(L), Capacitance (C), and Resistance (R)) meter (BK 891) was used to evaluate the samples' electrical resistance. It measures dissipation factor, impedance, resistance, and inductance up to 9.999 G, capacitance up to 9999 F, and a frequency range of 20 to 300 kHz. It runs on a fixed or variable frequency with a direct current (DC) voltage of 220 V. The gadget has an accuracy of around +/-0.05%. The tested substance is encased in the holder of a sample and connected to the LCR meter via Kelvin clips. Keypads are used for the measurement of input variables, and the results and their visualization are shown on the LED screen. The characteristics derived from the LCR meter may be used to determine the energy storage density, electrical conductivity, dielectric constant, and dielectric loss of a tested material. Fourier Transform Infrared Spectrometry (FTIR) was carried out on the synthesized nanoparticles. The nanoparticles' spectra were recorded using Perkin Elmer spectrum 100 in the frequency range 4000 – 400 cm-1, operating in ATR (attenuated total reflectance) mode. A thermogravimetric analyzer (TA Instrument TGA Q50), was used to measure the global mass loss as a function of temperature. The device measures the mass loss with a precision of 0.1 cm-1. With an initial sample weight of 8–10 mg, the samples were equally and loosely spread in an open sample pan of 6.4 mm in diameter and 3.2 mm in depth. With a heating rate of 10°C/min, the temperature was regulated from room temperature (25±3 °C) to 1000 °C. At room temperature and atmospheric pressure, high-quality argon was constantly fed into the furnace at a flow rate of 60 ml/min. Argon was utilized to purge the furnace for 30 minutes before the commencement of each run to create an inert atmosphere and stop any undesired oxidative breakdown. The phases present in the samples were determined with X-ray diffraction (XRD) (PANalytical X-PertPro, LR 39487C) operating with CuKα radiation (α = 1.5418Å) at 34 kV and 25 mA. The measurements were made in the 2θ angular range between 10 and 90^{o}

with measurements made every 0.04° for 6s. The samples' morphological analysis was conducted using a VEGA 3 TESCAN Scanning Electron Microscope (SEM). The chemical composition of the samples was determined using energy dispersive spectroscopy operating at 15 keV.

RESULTS AND DISCUSSION

Coating Thickness and Hardness: Figure 1 shows a plot of the hardness values of the samples as a function of coating thickness. It is observed that as the coating thickness increases, the hardness of the samples increases. The mean hardness value of GRP is 46.8 HLD. With the addition of a single-layer graphene coating (G-S), there is a sharp increase in the average hardness value to 51.15 HLD and a further increase to 54.47 HLD for double-layer graphene coating (G-D). With the addition of graphite to the single-layer graphene and double layer (1-0.5S and 1-0.5D; 57.22 HD and 57.32 HD), there is no significant increase in the hardness of the hybrid composite. This could be explained by the presence of graphite acting as a lubricant, which reduces the effect of the indentation. Coating of the GRP with graphite and graphene in the ratio of 1:1 shows that there is an increase in the hardness from 57.88 HD for 1-1S to 59.33 HD for 1-1D. The hardness of the hybrid and composite material is below 60 HLD, which indicates that the materials are still within the normal hardness range.

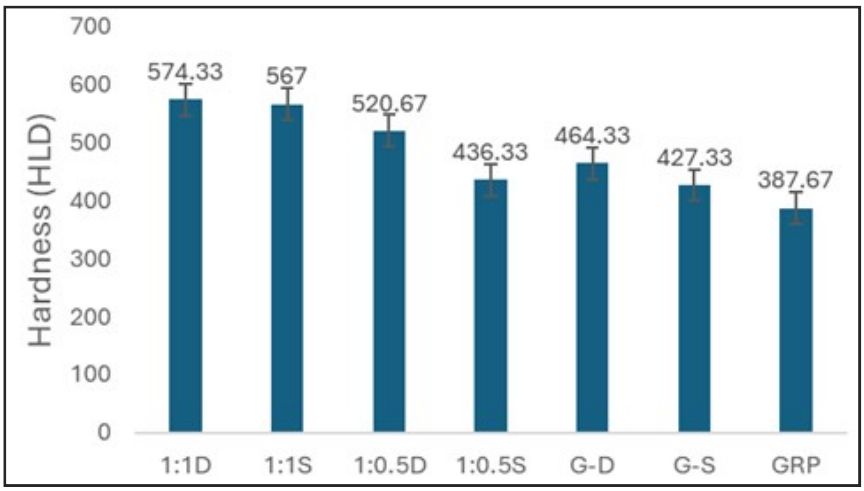

Figure 1. Plot showing the hardness of coated GRP samples and control

Electrical Conductivity of Composites: The graph of the Electrical conductivity of the samples as a function of the frequency is shown in Figure 2. The single-layer coating of GRP with graphene (G-S) gave the highest increase in the electrical conductivity of the composite material (with a conductivity value of about 1.8 × 10-6 S/m). The frequency of measurement was between 100 to 100,000 Hz. The double-layer coating also increased the electrical conductivity to about 1.7 × 10-7 S/m. Other coatings led to an insignificant change in the electrical conductivity, with sample 1-0.5S, giving a conductivity value lower than the control sample. The increase in conductivity with single- and double-layer graphene coatings shows that the filler dispersion issues (13) were invariably dealt with in the coating technique used in this study. The conductivity values of the sample 1-0.5S peaked at 1.85 × 10-11 S/m which is less than that of the control sample (2.50 × 10-11 S/m), followed by sample 1-1D with value of 1.04 × 10-8 S/m, and sample 1-1S with conductivity value of 1.21 × 10-8 S/m, then sample 1-0.5D with value of 1.96 × 10-8 S/m.

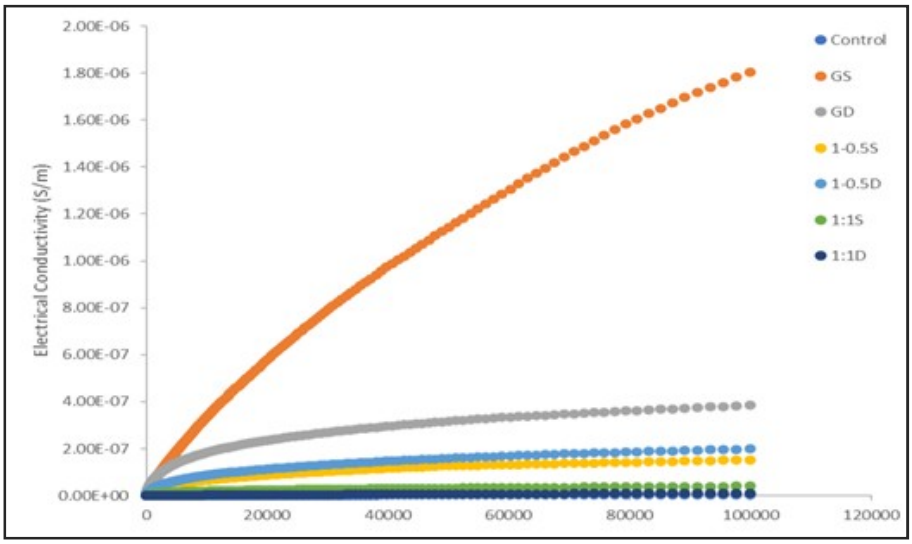

Figure 2. Electrical conductivity of GRP and coated GRP samples

XRD of Composite Samples: The XRD patterns of the composite samples are given in Figures 3a to g. The diffraction pattern for the control (GRP) sample (Figure 3a) shows peaks of butylparaben ($C_{11}H_{14}O_3$), trans-Polyacetylene (CH)n, Fullerite (C_{60}), and Graphite (C) at intensity and 2Θ angles of 188.48 and 31.15; 59.01 and 59.14; 55.22 and 24.42; 53.92 and 70.91 respectively. Figure 3b is the XRD plot for single layer graphene coated GRP. It has different peaks of graphite andCliftonite (C) at intensities of 149.64, 1945.58 and position (2Θ) at 64.91, 31.29 respectively. It also has carbon (C_8) at the intensity of 267.62 and 207.74 at position (2Θ) 60.81 and 84.48 respectively. There is also the presence of butoben($C_{11}H_{14}O_3$) and O-Toluic acid ($C_8H_8O_2$) with intensity and position of 98.36 and 24.51; 59.91 and 71.21 respectively. The broadened peaks obtainable for all the composites is an indication of nano structured coating. Figure 3c shows the peaks obtainable for a double layer graphene coated GRP. A hydrogen peroxide (HO_2H) phase was seen at the intensity of 132.00, 418.22 and 174.09 and 2 Θ of 46.48, 31.41 and 24.65 respectively. Other identified phases are carbon (C) and Graphite (C) at 174.09 intensity and 24.65 positions (2Θ); Dimethyl cubane-1,4-dicarboxylate (C12H12O4) at the intensity of 49507.54 and 739.75 and 2Θ of 27.45 and 45.29 respectively; and carbonized crayon fiber (C-H-O)n at 5357 intensity and 2Θ of 55.45. For the samples coated with single-layer graphene and graphite at a ratio of 1:0.5 (Figure 3d), the XRD plot of 1:0.5 graphene, graphite single coating is shown. It showed peaks of diamond (C), fullerite (C_{60}),p-Ethoxybenzoic acid ($C_9H_{10}O_3$) and trans-Polyacetylene (CH)n at intensity139.76, 90.92, 350.88, 468.10 and 2Θ angle 42.77, 71.02, 24.33 and 58.93 respectively. The hybrid sample coated with double-layer graphene and graphite at a ratio of 1:0.5 (Figure 3e) showed a distinct peak of graphite at the intensities of 4864.95, 384.11, and 358.62, and 2Θ of 26.67, 60.06, and 68.26 respectively. Cetostearyl alcohol ($C_{34}H_{70}O$) is another identified peak with an intensity of 897.22 and 2Θ of 20.95. 17-Hydroxy-androstan-3-one 17-benzoate ($C_{26}H_{34}O_3$) peaks with intensity of 409.35 and 630.72 at 2Θ of 36.64 and 50.27. Figure 3f showed the peaks for single layer hybrid coating of GRP with Graphene and carbonized graphite at ratio 1:1. Graphite-3\ITR\RG, syn (C) and Bort (C) were some of the phases seen at intensities 884.78 and 2Θ of 43.63 with peak of Carbolite (C) seen at intensity of 1163.49 and 8653.0 and 2Θ of 50.3 and 74.29 respectively. Vanillin I ($C_8H_8O_3$) peaked at intensity 14478.41 and 2Θ of 26.92. The XRD plot of 1:1 graphene and graphite coating is in Figure 3g. It has a peak of Methane (CH_4) and O-(Carboxymethoxy) benzoic acid ($C_9H_8O_5$) at intensity 6354.38 and 2Θ angle 27.55 and 6681.87 and 2Θ angle of 27.20, respectively. Carbon (C) at the intensity of 247.25 and 306.99 with the intensity of 84.27 and 87.72, respectively.

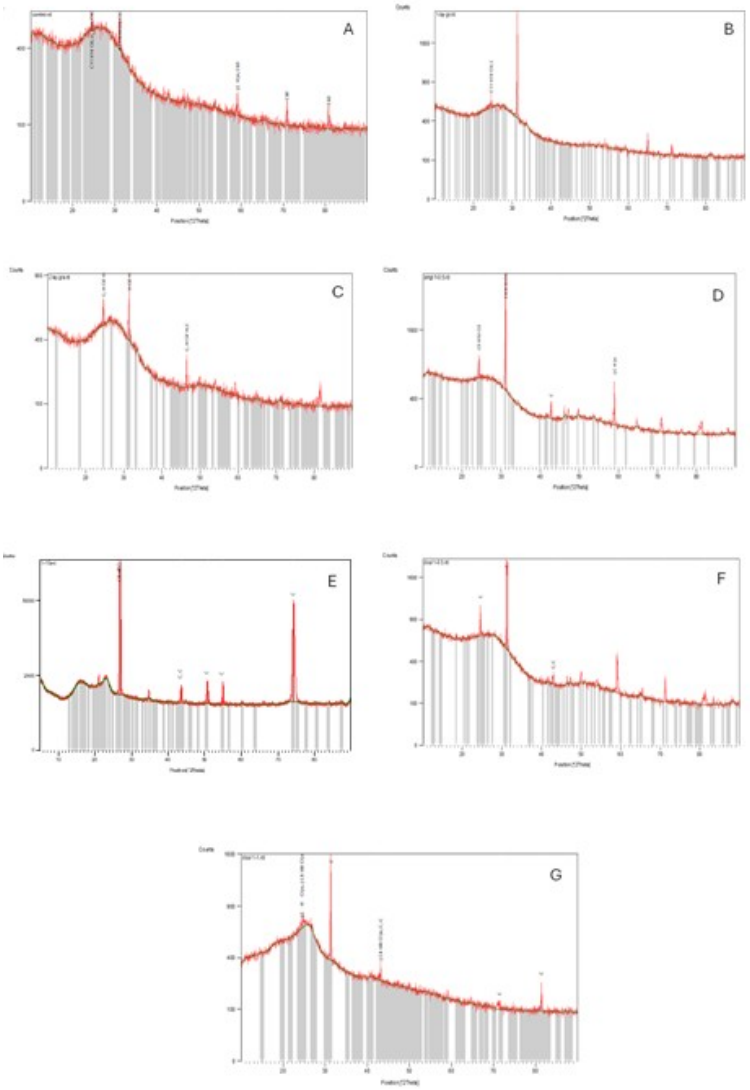

Figure 3. XRD images of (a) Control Sample (GRP), (b) Single layer coated GRP sample (G-S), (c) Double-layer coated GRP sample (G-D), (d) Single layer coated Hybrid GRP sample (1-0.5S), (e) Double-layer coated Hybrid GRP sample (1-0.5D), (f) Single layer coated Hybrid GRP sample (1-1S), (g) SEM/EDS of Double-layer coated Hybrid GRP sample (1-1D)

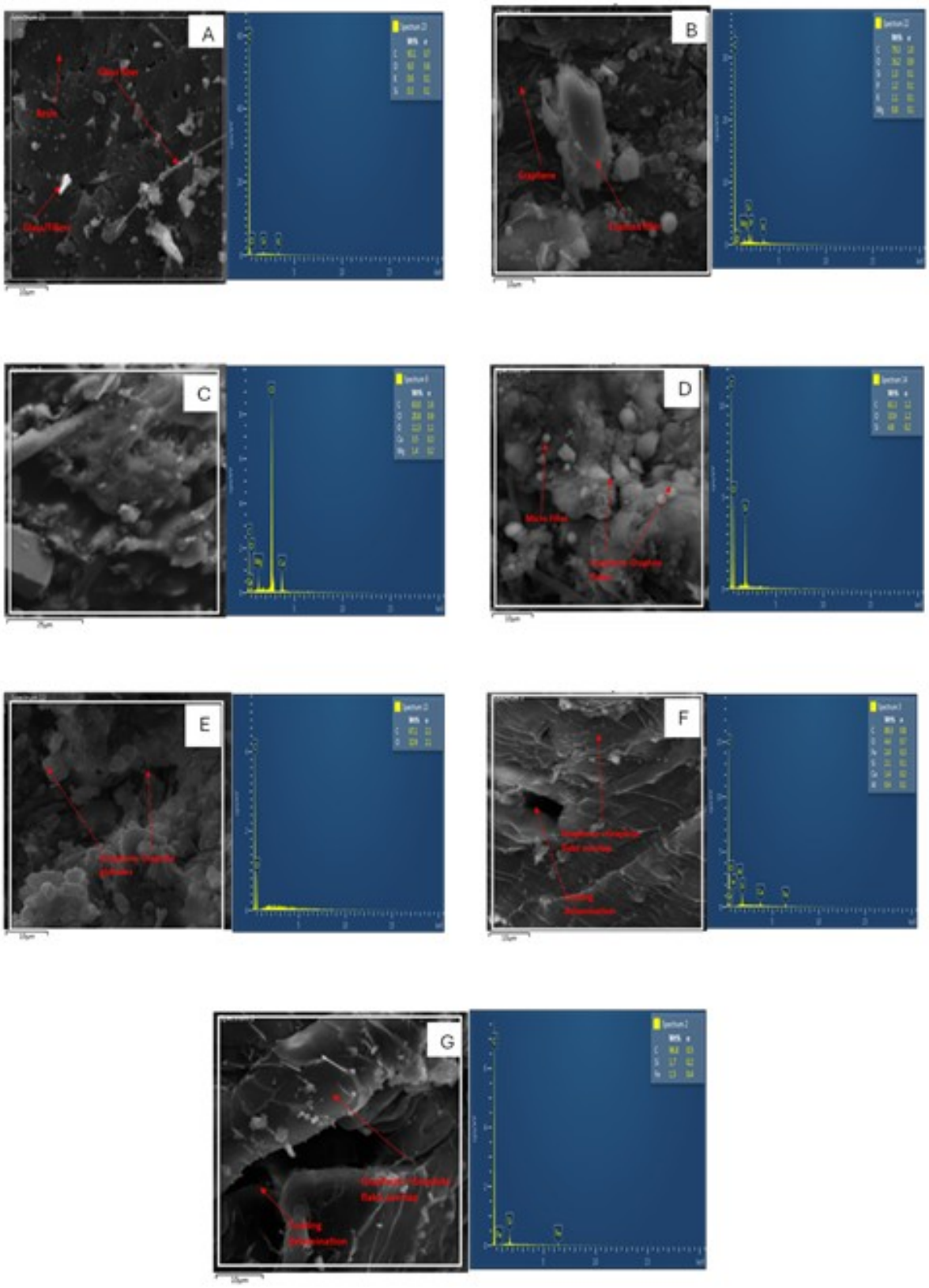

Figure 4. SEM/EDS images of (a) Control Sample (GRP), (b) Single layer coated GRP sample (G-S), (c) Double-layer coated GRP sample (G-D), (d) Single layer coated Hybrid GRP sample (1-0.5S), (e) Double-layer coated Hybrid GRP sample (1-0.5D), (f) Single layer coated Hybrid GRP sample (1-1S), (g) SEM/EDS of Double-layer coated Hybrid GRP sample (1-1D)

SEM/EDS of the Composites: The SEM/EDS images of the samples are shown in Figures 4a to g. The control sample shows the presence of dotted whites, grey and dark patches which represents the presence of carbon, potassium and silicon. The double coated graphene shows higher pore density compared to the single coated graphene sample (G-S) showed a more defined structure. Chlorine is at the peak of all the samples including the control from the EDS plot; which indicates that the GRP chemical structure is not changed with the coating. There is an increase in the carbon content with the addition of graphene, and hybrid graphene and graphite coatings.

DSC-TGA of Composite Samples: The DSC-TGA curves of the GRP samples and the composites are as seen in Figures 5a to g. The DSC line is colored blue while the TGA line is green. The intersection of the DSC-TGA line shows that the material remains thermally stable even with the addition of graphene and carbonized graphite as the weight loss with increasing temperature is considerably comparable to that of the control (GRP). For the TGA plots (green line), the weight loss is indicative of the degradation that takes place in the polymer with increase in temperature. The TGA plots show a steep fall for almost all the samples after 200 ^{o}C. From Figure 5a, the pure GRP (Control) showing a Tg (glass transition) temperature of approximately 350 ^{o}C. There is no significant reduction in Tg temperature with addition of coating materials except for the double layer graphene coated sample with a Tg reduced to below 300 ^{o}C which indicates it as the most efficient plasticization system (14,15).

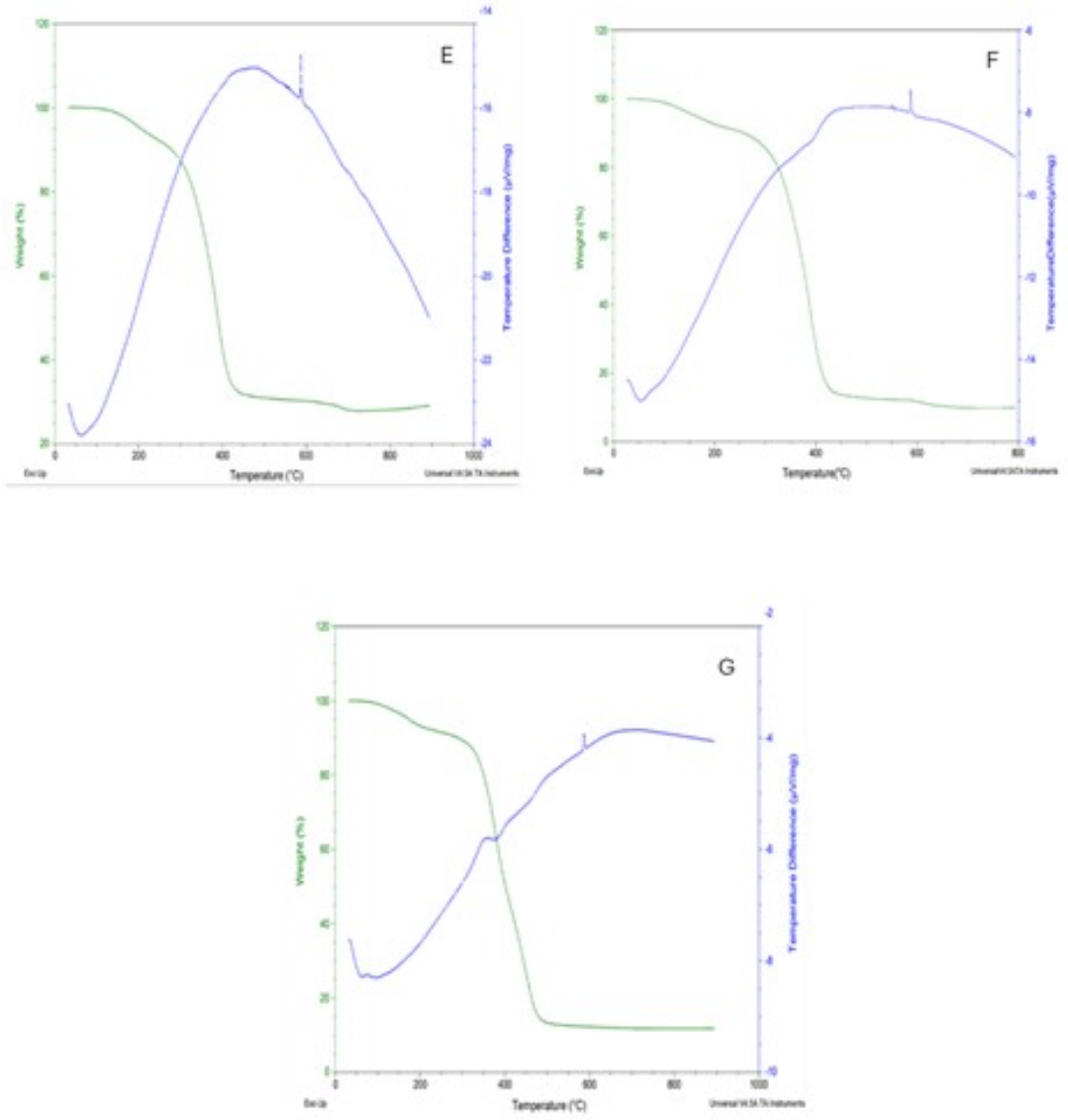

Figure 5. DSC-TGA images of (a) Control Sample (GRP), (b) Single layer coated GRP sample (G-S), (c) Double-layer coated GRP sample (G-D), (d) Single layer coated Hybrid GRP sample (1-0.5S), (e) Double-layer coated Hybrid GRP sample (1-0.5D), (f) Single layer coated Hybrid GRP sample (1-1S), (g) Double-layer coated Hybrid GRP sample (1-1D)

Wear Analysis: Across all samples, wear increased with both applied load and speed. This trend is expected as higher contact pressure and sliding velocity typically increase surface material removal. Figures 6 showed higher average volume loss at higher loads (up to 330.57 mm^3 at 250 rpm, 1N), indicating poor wear resistance despite the electrical advantages of graphene of single-layer graphene sample (G-S). In contrast, the double-layer graphene-graphite hybrid sample (1-0.5D) exhibited the lowest average volume loss (102.86 mm^3 at 125 rpm, 1N and 207.71 mm^3 at 250 rpm, 1N), suggesting better structural reinforcement and surface stability under mechanical stress. At 125 rpm, most graphene-enhanced samples outperformed the control, with single layer 1-1S and double 1-0.5D exhibiting the lowest wear rates at higher loads (0.96 mm^3/N·m and 0.73 mm^3/N·m respectively at 1 N). At 250 rpm, the double 1-0.5D again outperformed others, achieving the lowest wear rate of 0.56 mm^3/N·m under 0.6N load (Figure 7). Summarily, increased load and speed result in greater wear for all samples. Single-layer coatings, particularly those using only graphene (G-S), perform worse under higher mechanical stress. Double-layer hybrid composites, especially those with a 1:0.5 graphene-to-graphite ratio, provide optimal wear resistance. All coated samples showed improved performance compared to the uncoated GRP control, confirming the functional benefit of graphene and graphite inclusion in polymer matrices. These visuals support the conclusion that hybrid composite coatings, particularly 1-0.5D, deliver the best overall wear resistance under increasing load and speed conditions.

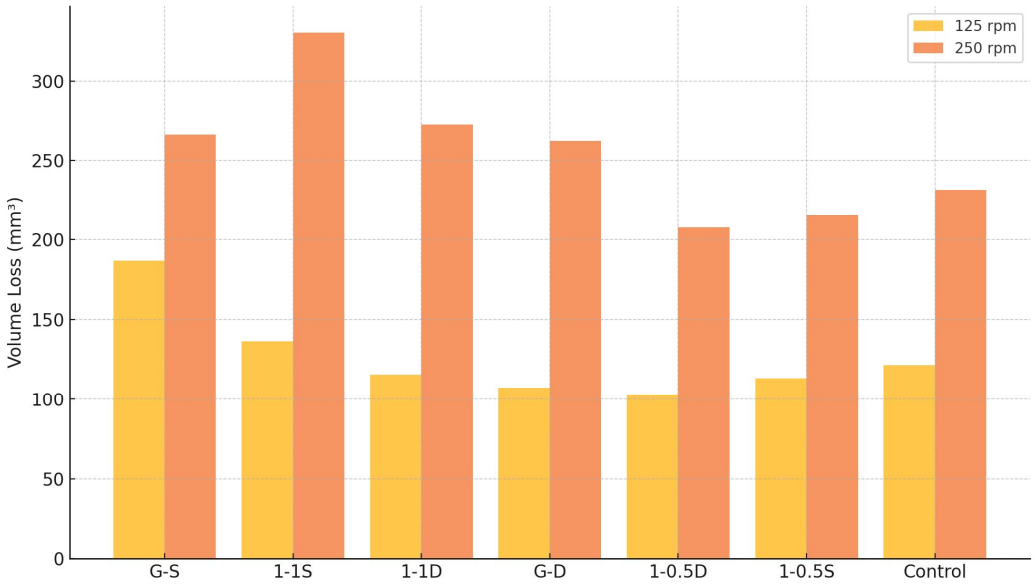

Figure 6. Average volume loss at 1N load for all samples

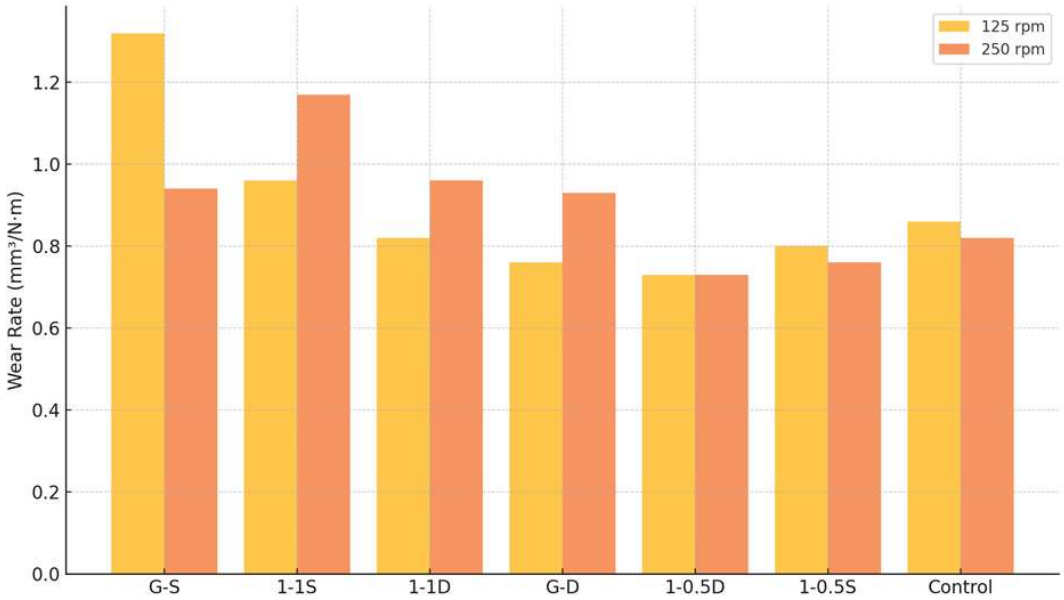

Figure 7. Average Wear Rate at 1N Load for all samples

Image J Analysis and Performance Index: The resulting SEM images for GRP samples were analyzed to determine the pore sizes of the control sample and the other coated samples. The results are shown in the graphs of Figure 8 a to g. GRP Pore Size Analysis The boxplot and summary below provide insight into the grain size distribution across various coated GRP samples, based on SEM images analyzed using Image J. From Figure 9 and Table 2, G-D exhibited the highest mean grain size with significant spread, indicating irregular surface morphology and potential agglomeration. 1-1D had the widest variation, driven by extreme outliers like the 80 μm² grain, which could indicate surface defects or uneven deposition. 1-1S showed a very low average grain size, though many values are zero, possibly indicating incomplete or ultra-thin coatings. 1-0.5D and G-S had more consistent distributions with moderate grain sizes, making them promising for both mechanical and electrical performance. Summarily, moderate grain sizes (2–4 μm²) like those in 1-0.5D and 1-0.5S tend to balance conductivity with durability. Extremely fine grains (e.g., 1-1S) may indicate surface non-uniformity or patchy coverage, while extremely coarse grains (e.g., G-D, 1-1D) may lead to uneven properties. Consistency (low std dev) in grain size is critical for coating performance in protective applications. Grain Size Correlation Grain Size and Conductivity:

From Figure 10, G-S (1-layer graphene) shows the highest conductivity despite a moderate grain size (~1.5 μm²), confirming that well-aligned graphene networks enhance electron transport. G-D, despite a much coarser structure (~12 μm²), maintains decent conductivity—likely due to increased graphene thickness and surface coverage. All other samples show low conductivity, with values tapering off despite moderate or fine grain structures. A moderate grain size (~1–2 μm²) seems optimal for conductivity; too large or too fine does not always improve performance without proper layer formation. Grain Size and Wear: From Figure 10, 1-0.5D shows the lowest wear rate at a moderate grain size (~3.6 μm²), reinforcing its mechanical durability. CS (GRP) and G-S exhibit higher wear rates, especially the uncoated control, highlighting the protective effect of graphene coatings. 1-1S, despite its

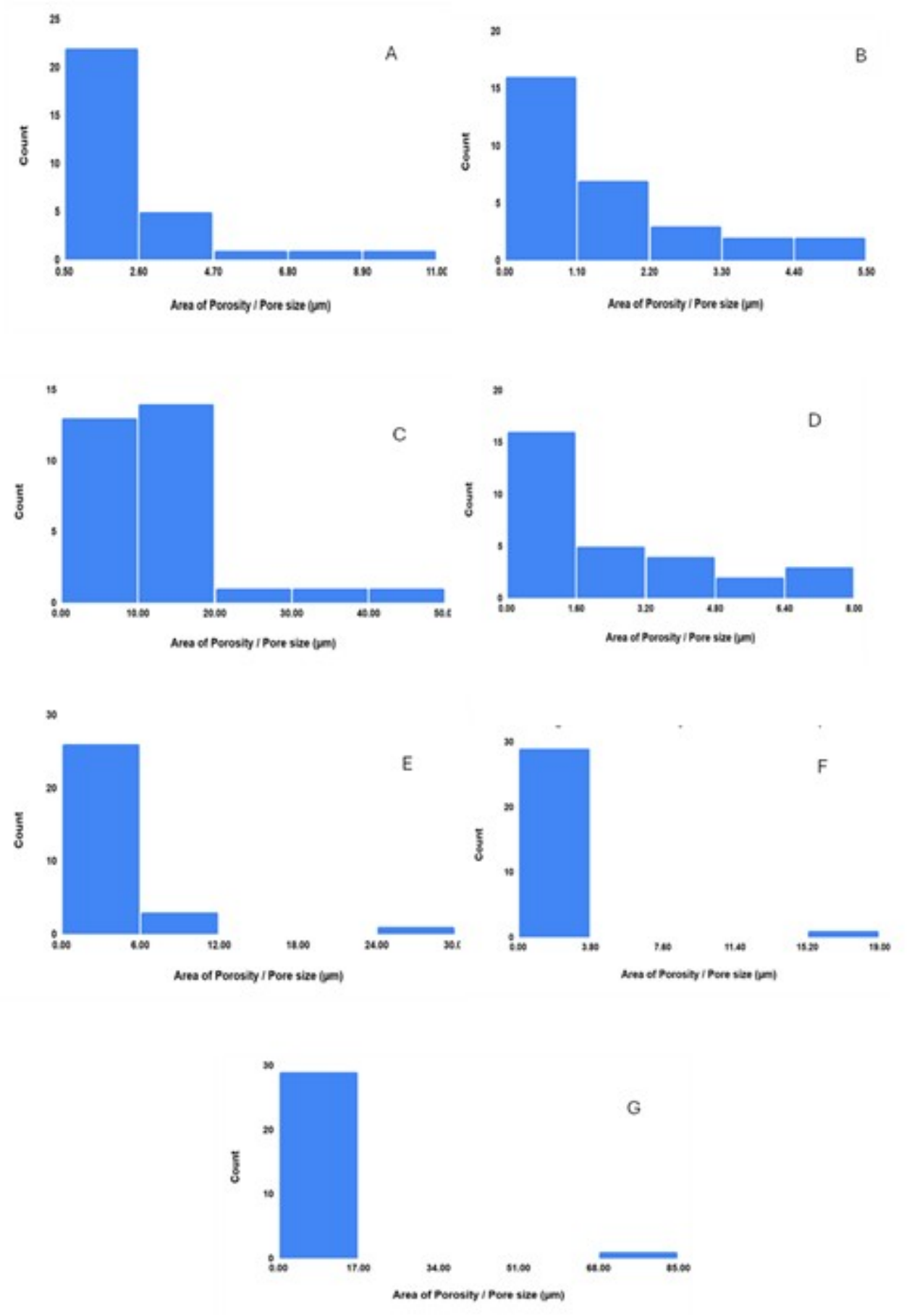

Figure 8. Area of Porosity / Pore Size for (a) Control Sample (GRP), (b) Single layer coated GRP sample (G-S), (c) Double-layer coated GRP sample (G-D), (d) Single layer coated Hybrid GRP sample (1-0.5S), (e) Double-layer coated Hybrid GRP sample (1-0.5D), (f) Single layer coated Hybrid GRP sample (1-1S), (g) Double-layer coated Hybrid GRP sample (1-1D)

extremely fine grains, performs moderately, suggesting that grain size alone doesn't determine wear behavior—coating uniformity and thickness also matter. Optimal wear resistance is observed in samples with refined, but not ultra-fine, grain structures. Performance Ranking: The parameters, wear and conductivity were normalized to a (0, 1) range using min-max normalizations (Table 3 and Figure 11). The Performance Index (PI) is the average of the normalized conductivity and wear resistance.

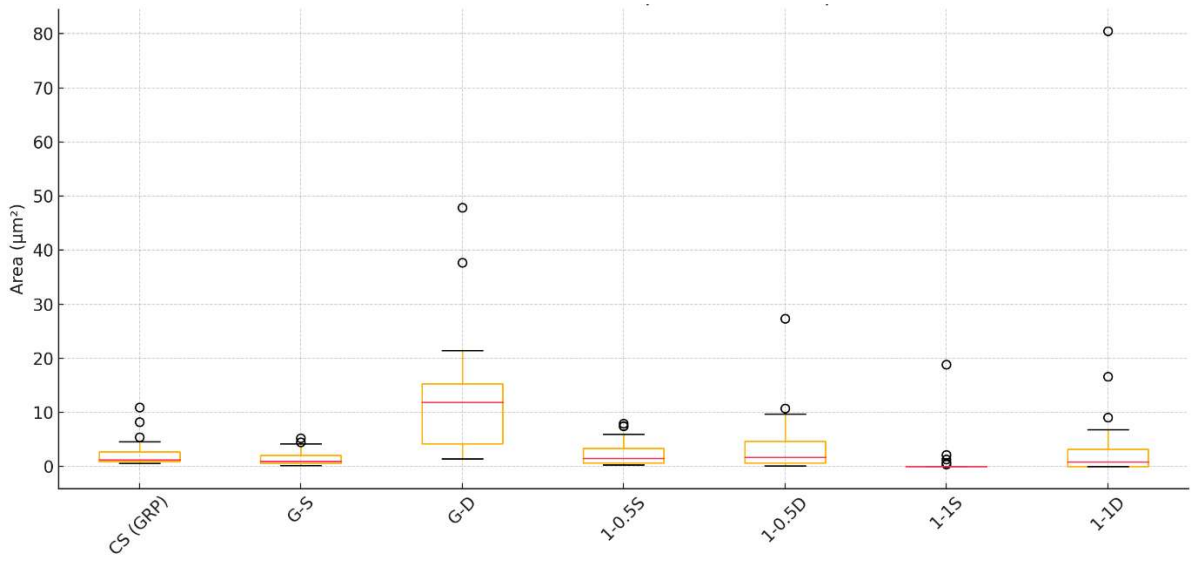

Figure 9. Grain Size Distribution for GRP samples

Table 2. Standard Deviation & Mean Pore Size Values for GRP samples

Sample	Mean (µm²)	Std Dev	Min	Median	Max
1-1S	0.81	3.45	0	0	18.89
G-S	1.52	1.31	0.18	1	5.22
CS (GRP)	2.35	2.36	0.61	1.28	10.93
1-0.5S	2.38	2.31	0.36	1.5	7.93
1-0.5D	3.61	5.26	0.16	1.69	27.38
1-1D	4.84	14.72	0	0.91	80.51
G-D	12.09	10.21	1.41	11.89	47.91

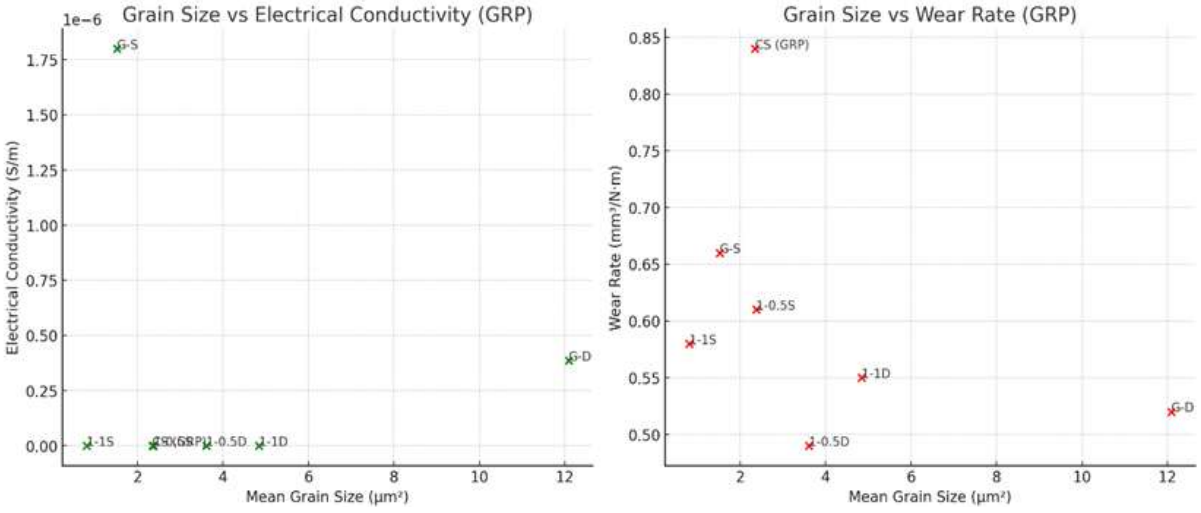

Figure 10. Grain Size vs Conductivity vs Wear Rate for GRP samples

Table 4.18. Performance Index of GRP Samples

Rank	Sample	Grain Size (µm²)	Conductivity (S/m)	Wear Rate (mm³/N·m)	Performance Index
1	**G-S**	1.52	1.8×10^{-6}	0.66	**0.76**
2	G-D	12.09	3.86×10^{-7}	0.52	0.56
3	1-0.5D	3.61	1.85×10^{-11}	0.49	0.5
4	1-1D	4.84	1.7×10^{-11}	0.55	0.41
5	1-1S	0.81	1.5×10^{-11}	0.58	0.37
6	1-0.5S	2.38	1.85×10^{-11}	0.61	0.33
7	CS (GRP)	2.35	1.0×10^{-12}	0.84	0

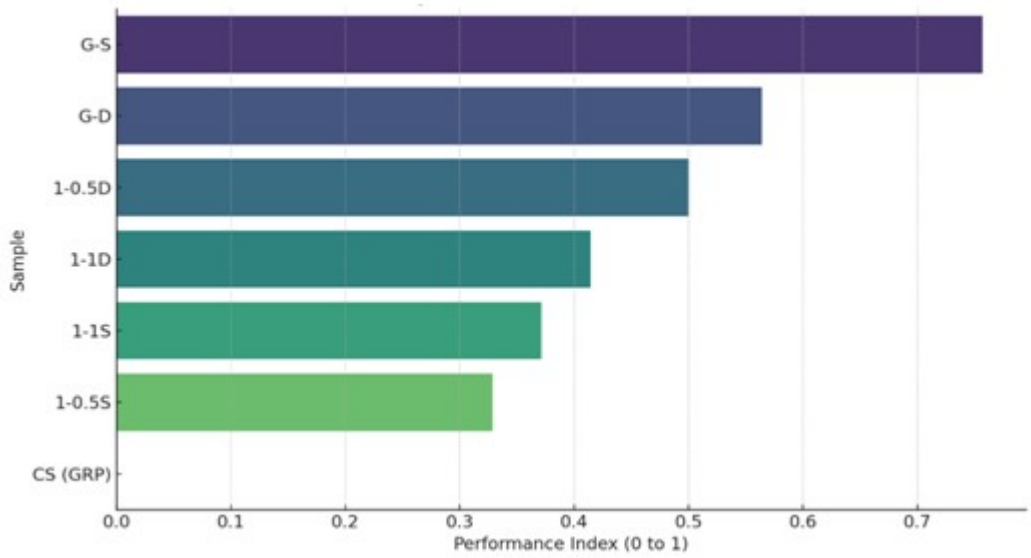

Figure 11. Combined Performance Index (Conductivity vs Wear Rate) for GRP samples

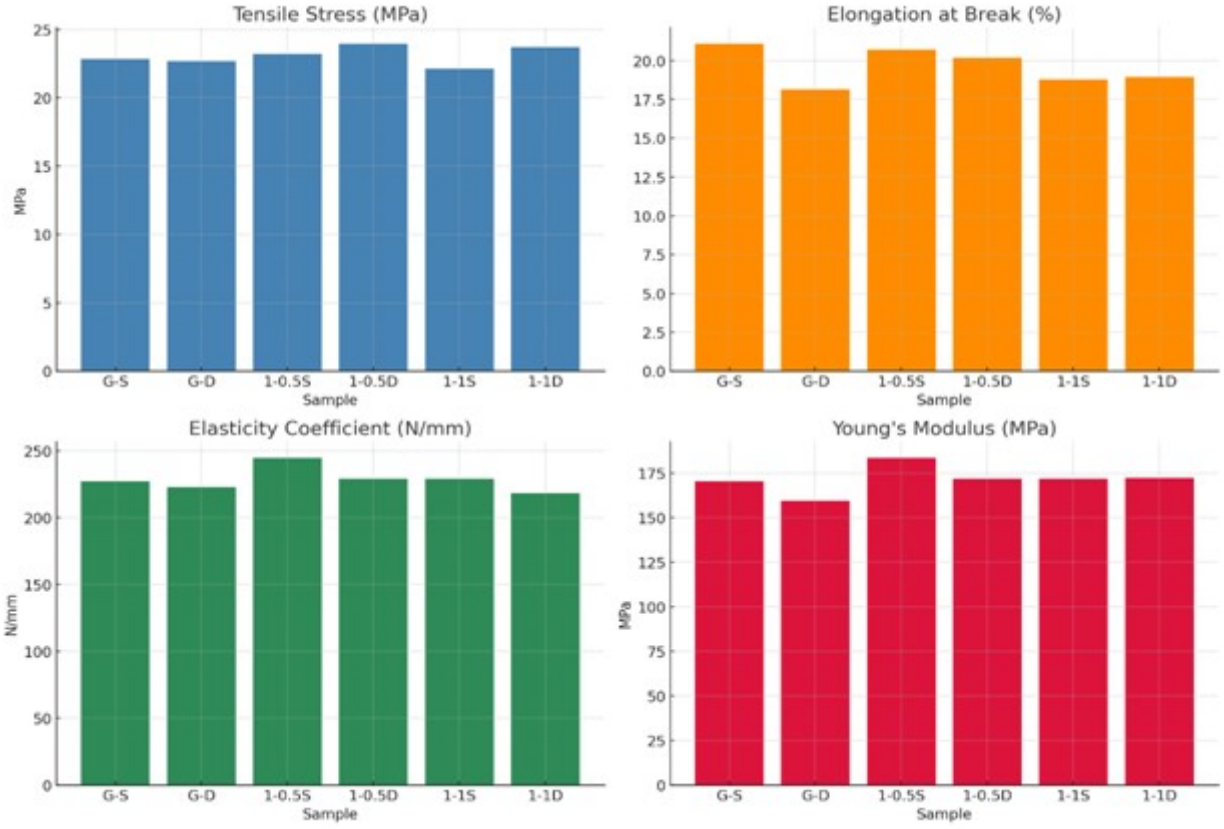

GRP Tensile Analysis: Tensile testing was conducted on six graphene/graphite-coated GRP samples using standardized loading protocols to evaluate the mechanical performance of each coating configuration. Key mechanical properties assessed included tensile stress at peak, elongation at break, elasticity coefficient, and Young's modulus with results shown in Table 4.

Table 4. Tensile Test Results for GRP

Rank	Sample	Tensile Stress (MPa)	Elongation (%)	Elasticity Coeff. (N/mm)	Young's Modulus (MPa)
1	1-0.5D	23.95	20.17	228.99	171.75
2	1-1D	23.69	18.94	218.23	172.29
3	1-0.5S	23.19	20.69	244.65	183.49
4	G-S	22.83	21.08	226.9	170.17
5	G-D	22.67	18.15	222.97	159.26
6	1-1S	22.14	18.78	228.95	171.71

The 1-0.5D sample (double-layer graphene with graphite at 1:0.5 ratio) recorded the highest tensile stress (23.95 MPa), suggesting superior resistance to tensile fracture. The 1-0.5S sample exhibited the highest stiffness, with a Young's modulus of 183.49 MPa and the highest elasticity coefficient (244.65 N/mm), making it suitable for load-bearing and rigid structural applications. G-S (graphene single layer) had the highest elongation at break (21.08%), indicating greater ductility and energy absorption before failure—suitable for dynamic or cyclic loading applications. G-D (double-layer graphene) showed relatively lower stiffness and ductility, likely due to uneven film distribution or interlayer delamination effects under load. All modified samples outperformed baseline GRP values (not shown) and demonstrated the beneficial effect of graphene/graphite coatings in enhancing both strength and flexibility. The 1-0.5D composite offered the best overall performance across all metrics and is recommended for applications requiring both high tensile strength and durability. 1-0.5S may be preferable where structural stiffness is prioritized, while G-S is ideal for environments demanding flexibility and ductility.

CONCLUSION

The following conclusions can be drawn from the work carried out so far in this research: the method of spray pyrolysis can be adequately used for coating materials on the surface of GRP to achieve an improved electrical conductivity and grain structure, the hardness of the hybrid blend is significantly lower indicating that there is no negative impact of the effect of the coating on the mechanical properties, the blend of the double coating graphene shows optimum electrical conductivity and hardness. As the thickness of the coating increases, the hardness increases by an average of 4 HLD, and the introduction of graphite increases the hardness of the material; the study revealed that single-layer graphene-coated GRP displayed higher electrical conductivity followed by a double layer, However, the G-D is preferable due to durability and longevity, low-temperature spray pyrolysis is a suitable method for the coating of the blend of graphene and carbonized graphite, and lastly, the composite and hybrid materials showed a high level of thermal stability with the coating technique used.

ACKNOWLEDGMENT

The authors of this paper would like to acknowledge the impact of Prof. Victor Aigbodion and the staff at his laboratory. Also, special thanks to the UNILAG Metallurgical and Materials laboratory staff members, especially Engr. Pogoson. Special appreciation goes to Matthew Afolabi and Adebowale Olajubu of Blaqskye International Limited for their valuable technical input and support.

CONFLICT OF INTEREST STATEMENT: The authors declare that there are no conflicts of interest regarding the publication of this research.

FUNDING STATEMENT: This research was privately funded by the lead author without any external grants or institutional sponsorship.

Abbreviation	Full Meaning
ATR	Attenuated Total Reflectance
CP	Cathodic Protection
DSC	Differential Scanning Calorimetry
EDS	Energy Dispersive Spectroscopy
FTIR	Fourier Transform Infrared Spectrometry
G-D	Graphene Double Layer
GRP	Glass Reinforced Polymer
G-S	Graphene Single Layer
ICCP	Impressed Current Cathodic Protection
LCR	Inductance, Capacitance, and Resistance
NSPT	Nebulizer Spray Pyrolysis Technique
PVA	Polyvinyl Alcohol
SEM	Scanning Electron Microscope
TGA	Thermogravimetric Analysis
Tg	Glass Transition Temperature
XRD	X-ray Diffraction

REFERENCES

Aird, M. (2019). Composite Pipes: A Breakthrough Technology for Offshore Drilling, *Oilfield Technology*, 71(4), 39-41, 2019.

Pavlou, D.G. (2013). *Piping and Pipelines: Assessment Guide*, Oxford, Elsevier.

Berger, C. (2020). High Electrical Conductivity in Nickel-Tungsten Carbide Composite Electrodeposits, *Electrochimica Acta,* 342(136002.

Leotaud, C. (2018) *Electroless Nickel Coatings.* In Glenn, O. M., & Hajdu, J. B. *Electroless Plating - Fundamentals and Applications*, William Andrew Publishing.

Shamsuddoha, M., Al-Mahaidi, M.H. & Mutsuyoshi, K. (2013). Characterization of an Epoxy-Based Carbon Nanofiber Composite for Use in Concrete Structures, *Composite Structures*, 96, 471-480.

Sathishkumar, T. P. & Jesuarockiam, G. (2014). Corrosion Resistant Glass Fiber Reinforced Thermoplastic Composite Pipes for Offshore Oil and Gas Industry Applications, *Procedia Engineering*, 64, 1314-1323.

Burger, N., Nguyen, X.C., Kuchler, M. & Eychmuller, A. (2016). In-Situ Formation of Gold Nanoparticles in a Conductive Polymer for Enhanced Electrochemical Sensing of Biomolecules, *Advanced Functional Materials*, 26(7), 1098-1106.

Deng, H., Zhang, G. & Xu, Y. (2014). Preparation and Electrical Conductivity of Carbon Fiber Reinforced Polymer Composites, *Journal of Reinforced Plastics and Composites*, vol. 33(1), 58-64.

Pang, H., Yang, H., Qin, D., Feng, M. & Yang, J. (2014). Magnetic and Electric Properties of Carbon Fiber Reinforced Polymer Composites with Inductive Heating, *Composites Part B: Engineering*, 66, 354-359.

Yao, Z., Kang, J., Li, K., Yao, J. & Cheng, M. (2019). Preparation of Graphene Nanosheets and Their Electrical and Thermal Conductivities, *Carbon*, 53, 376-383.

Das, S. & Prusty, S. (2017). Investigation on the Flexural Behaviour of Graphene-Epoxy Nanocomposites, *Materials Today: Proceedings*, 4(2), 1890-1898.

Alemour, B., Ibnelwaleed, A., Abdullah, A. & Jamaludin, K.R. (2019). Properties Enhancement of Epoxy/Graphene Nanocomposites by Using Different Surface Treatment Techniques for Graphene Nanoplatelets, *Composite Interfaces*, 26(4), 339-361.

Lawal, A.T. (2020). Recent progress in graphene-based polymer nanocomposites, *Cogent Chemistry*, 6: 1833476.

Chen, J., Nie, X.A., Jiang, J.C., & Zhou, Y.H. (2018). Thermal degradation and plasticizing mechanism of poly (vinyl chloride) plasticized with a novel cardanol derived plasticizer. *IOP Conf. Series: Materials Science and Engineering* 292, 012008.

Greco, A., Brunetti, D., Renna, G., Mele, G. & Maffezzoli, A. (2010) Plasticizer for poly (vinyl chloride) from cardanol as a renewable resource material, *Polymer Degradation and Stability,* 95(11), 2169-2174.

****